Articles in PresS. Am J Physiol Heart Circ Physiol (February 13, 2009). doi:10.1152/ajpheart.01206.2008

Rho-Kinase-Mediated Suppression of K_{DR} Current in Cerebral Arteries Requires an Intact Actin Cytoskeleton

Kevin D. Luykenaar, Rasha Abd El-Rahman, Michael P. Walsh[1], and Donald G. Welsh

Dept. of Physiology & Biophysics, University of Calgary, Alberta, Canada

[1]Dept. of Biochemistry and Molecular Biology, University of Calgary, Alberta, Canada

Running Title: Rho-kinase and K_{DR} current

Key Words: Pyrimidine nucleotides, Rho signaling, Potassium channels, Vascular smooth muscle

Corresponding Author:

Donald G. Welsh, Ph.D.
Smooth Muscle Research Group
HMRB-G86, Heritage Medical Research Building
University of Calgary
3330 Hospital Dr. N.W.
Calgary, Alberta, Canada, T2N 4N1

Phone: (403) 220-3819
Fax: (403)-220-3820
Email: dwelsh@ucalgary.ca

ABSTRACT

This study examined the role of the actin cytoskeleton in Rho-kinase-mediated suppression of the delayed rectifier K^+ (K_{DR}) current in cerebral arteries. Myocytes from rat cerebral arteries were enzymatically isolated and whole cell K_{DR} currents monitored using conventional patch clamp electrophysiology. At +40 mV, the K_{DR} current averaged 19.8 ± 1.6 pA/pF (mean ± SE) and was potently inhibited by uridine triphosphate (UTP; 3×10^{-5} M). This suppression was observed to depend on Rho-signaling and was abolished by the Rho-kinase inhibitors H-1152 (3×10^{-7} M) and Y-27632 (3×10^{-5} M). Rho-kinase was also found to concomitantly facilitate actin polymerization in response to UTP. We therefore examined whether actin dynamics played a role in the ability of Rho-kinase to suppress K_{DR} current and found that actin disruption using either cytochalasin D (1×10^{-5} M) or latrunculin A (1×10^{-8} M) prevented current modulation. Consistent with our electrophysiological observations, both Rho-kinase inhibition and actin disruption significantly attenuated UTP-induced depolarization and constriction of cerebral arteries. We propose that UTP initiates Rho-kinase-mediated remodeling of the actin cytoskeleton and consequently suppresses the K_{DR} current, thereby facilitating the depolarization and constriction of cerebral arteries.

INTRODUCTION

A network of resistance arteries controls the distribution of blood flow through the cerebral circulation. Arterial tone is determined by smooth muscle contractility and is regulated by a number of physiological factors, including metabolic state (9), humoral and neural stimuli (27), intraluminal pressure (10; 17), as well as endothelial factors (16). Many of these stimuli initiate changes in vascular tone via G-protein coupled receptors and the activation of downstream signaling pathways. Effector proteins within such transduction pathways can influence vascular smooth muscle contractility by altering the Ca^{2+} sensitivity of the myofilaments (29) and/or the activity of ion channels that control membrane potential and voltage-gated Ca^{2+} entry (22).

The Rho pathway is a primary signaling pathway regulating vascular smooth muscle contraction. Rho signaling is initiated via receptors coupled to $G_{12/13}$, resulting in the activation of the small GTPase RhoA and its principal downstream effector, Rho-kinase (3; 28). Rho-kinase directly phosphorylates and inactivates myosin light chain phosphatase (MLCP), ultimately increasing the phosphorylation state of myosin and facilitating contraction (30). Recent studies suggest that Rho-kinase is also capable of modulating ion channels and membrane potential (8; 19). In particular, we found that Rho-kinase was essential to the depolarization and constriction of cerebral arteries in response to agonists such as uridine triphosphate (UTP). Electrophysiological measurements revealed that depolarization involved the Rho-mediated inhibition of a delayed rectifying K^+ (K_{DR}) current (19).

The mechanism by which Rho-kinase suppresses the K_{DR} current remains unclear. One possibility is that Rho-kinase may directly phosphorylate K_V channels underlying the K_{DR} current to reduce open probability. Currently, however, there is no experimental evidence in support of such a mechanism. Alternatively, Rho-kinase may indirectly mediate K_{DR} channel suppression by targeting the actin cytoskeleton. A number of vascular studies have implicated Rho-kinase in remodeling of the actin cytoskeleton, where it facilitates the polymerization of actin structures (1; 5; 33). Examination of the signaling events underlying this process has revealed that Rho-kinase likely phosphorylates and activates LIM-kinase, an endogenous inhibitor of cofilin, a protein that catalyzes the disassembly of filamentous actin (12). Intriguingly, past studies have demonstrated that both Kv1.2 and Kv1.5, key pore forming subunits of the cerebral arterial K_{DR} current, can couple to actin via the cytoskeletal-binding proteins cortactin and α-actinin2, respectively (11; 21). In consideration of these observations, it

is conceivable that Rho-kinase may regulate K_{DR} current by modifying cytoskeletal elements to influence channel activity, thereby producing the electrical and vasomotor responses associated with the constriction of cerebral arteries.

In this study, we examined the roles of Rho signaling and the actin cytoskeleton in enabling vasoconstrictors to suppress the K_{DR} current and elicit arterial depolarization. Electrophysiological measurements confirmed that the K_{DR} current was potently inhibited by UTP through a mechanism dependent on Rho-kinase. We found that Rho-kinase facilitated actin polymerization in response to UTP, and that a functional actin cytoskeleton was necessary for K_{DR} current suppression. Furthermore, disrupting the actin cytoskeleton limited the ability of UTP to depolarize and constrict cerebral arteries, similar to the effects of Rho-kinase inhibition. Our findings suggest that Rho-kinase likely modifies actin cytoskeletal structure to reduce K_{DR} channel activity, thereby facilitating the depolarization and constriction of cerebral arteries.

MATERIALS AND METHODS

Animal procedures and tissue preparation. Animal procedures were approved by the University of Calgary Animal Care and Use Committee. Female Sprague-Dawley rats (10-12 weeks of age; ~150 grams) were euthanized via carbon dioxide asphyxiation. Following euthanasia, the brain was isolated and stored in ice-cold phosphate-buffered (pH 7.4) saline solution containing (in mM): 138 NaCl, 3 KCl, 10 Na_2HPO_4, 2 NaH_2PO_4, 5 glucose, 0.1 $CaCl_2$, and 0.1 $MgSO_4$. Middle cerebral arteries were carefully dissected free of connective tissue and cut into ~2 mm segments.

Isolation of arterial smooth muscle cells. Middle cerebral arteries were enzymatically digested to isolate smooth muscle cells. In brief, arterial segments were equilibrated for 10 minutes at 37°C in an isolation medium containing (in mM): 60 NaCl, 80 Na-glutamate, 5 KCl, 2 $MgCl_2$, 10 glucose, and 10 HEPES with 1 mg/ml albumin (pH 7.4). Tissue samples were subsequently incubated for 15 minutes in the same medium supplemented with 0.5 mg/ml papain and 1.5 mg/ml dithioerythritol, followed by a 10 minute incubation in medium containing 100 µM Ca^{2+}, 0.7 mg/ml type F collagenase, and 0.4 mg/ml type H collagenase. The tissue was then washed repeatedly in ice-cold isolation medium and triturated with a fire-polished pipette to disperse smooth muscle cells. Cell samples were stored in cold isolation medium for electrophysiological study the same day.

Electrophysiology. Conventional patch clamp electrophysiology was used to measure K_{DR} currents as previously described (20). Patch pipettes were pulled from borosilicate glass and fire-polished to resistances of 4-7 MΩ. Pipettes were then coated with wax to reduce capacitance and backfilled with pipette solution containing (in mM): 110 K^+-gluconate, 30 KCl, 0.5 $MgCl_2$, 5 HEPES, 10 EGTA, 5 Na_2-ATP, and 1 GTP (pH 7.2). Cells were voltage clamped in a bath solution containing (in mM): 120 NaCl, 3 $NaHCO_3$, 4.2 KCl, 1.2 KH_2PO_4, 2 $MgCl_2$, 0.1 $CaCl_2$, 10 glucose, and 10 HEPES (pH 7.4). A 1 M NaCl-agar salt-bridge around the reference electrode was used to minimize offset potentials. Whole-cell currents were recorded on an Axopatch 200B amplifier (Molecular Devices, MDS Analytical Technologies, Mississauga, ON), filtered at 1 kHz, digitized at 5 kHz, and analyzed with Clampfit 8.2 software. Cell capacitance was measured with the cancellation circuitry in the voltage-clamp amplifier and averaged 16.8 ± 0.7 pF. All experiments were performed at room temperature (20-22^{o}C). Cells were voltage-

clamped at -60 mV and equilibrated for 15 minutes prior to experimentation. Whole-cell K_{DR} currents were monitored under control conditions and following the addition of UTP (3×10^{-5} M). To examine Rho-kinase signaling and the function of the actin cytoskeleton, myocytes were preincubated in H-1152 (3×10^{-7} M), Y-27632 (3×10^{-5} M), cytochalasin D (1×10^{-5} M), or latrunculin A (1×10^{-8} M) prior to the addition of UTP. In several experiments, 5×10^{-3} M 4-aminopyridine (4-AP) was used to ascertain the magnitude of the 4-AP-sensitive K_{DR} current. In general, the net current-voltage relationship was determined by measuring peak current at the end of 300 ms voltage commands ranging from -70 to +40 mV. Following each pulse, a voltage step to -40 mV was used to monitor tail currents for analysis of steady-state activation.

Arterial diameter and E_m. Segments of unbranched middle cerebral arteries (~2 mm in length) were cannulated and mounted in a customized arteriograph chamber (J.B. Pierce Laboratory, New Haven, CT) and superfused with warm (37°C) physiological salt solution (PSS; pH 7.4) containing (in mM): 119 NaCl, 4.7 KCl, 20 $NaHCO_3$, 1.7 KH_2PO_4, 1.2 $MgSO_4$, 1.6 $CaCl_2$, and 10 glucose. Arteries were maintained under no flow conditions and at low intraluminal pressure (15 mmHg) to minimize myogenic mechanisms during the examination of agonist responses. Endothelial-dependent mechanisms were eliminated by passing air bubbles through the arterial lumen. Arterial diameter was monitored using an automated edge detection system (IonOptix, Milton, MA). Smooth muscle E_m was recorded by inserting a glass microelectrode (120-150 MΩ) filled with 1 M KCl into the vessel wall and assessing the voltage difference across the membrane using an intracellular electrometer (Warner Instruments, Hamden, CT). Successful cell impalements consisted of: 1) a sharp negative E_m deflection upon entry, 2) a stable recording following entry, and 3) a sharp return to baseline upon electrode removal. Cerebral arteries were equilibrated for 30 minutes at 37°C prior to experimentation. Prior to experimentation, the contractile ability of each vessel was determined by a brief exposure to KCl (6×10^{-2} M). To ascertain whether Rho-kinase and the cytoskeleton were involved in UTP-induced constriction, changes in arterial diameter and smooth muscle E_m were measured under control conditions, in response to UTP, and following the addition of H1152, cytochalasin D, or latrunculin A.

Actin polymerization. Arterial segments were stripped of endothelium and placed in physiological salt solution. Following treatment with UTP and/or H-1152, G- and F-actin

were separated by centrifugation and detected using a commercially available kit (Cytoskeleton, Denver, CO). Briefly, arteries were homogenized and centrifuged at low speed (2,000 rpm) for 5 minutes to spin down unbroken cells and debris. The supernatant was centrifuged at high speed (100,000 g for 60 min at 37°C) to separate F-actin (pellet) and G-actin (supernatant). F-actin was resuspended in 200 µl of ice-cold water and depolymerized using 10 µM cytochalasin D. Samples were then diluted in 4x SDS sample buffer and heated to 95°C for 2 minutes. Equal volumes of G- and F-actin samples were subsequently separated on a 12% polyacrylamide gel. Proteins were transferred to polyvinylidene difluoride membranes and probed with rabbit anti-actin polyclonal antibody and HRP-conjugated anti-rabbit secondary antibody. Proteins were visualized by chemiluminescence and quantified using Fujifilm Multigauge3.1 software. G-actin was additionally quantified with respect to SM22. Actin blots were re-probed using goat anti-SM22 antibody and HRP-conjugated anti-goat secondary antibody. SM22 was subsequently visualized, quantified, and used to standardize G-actin content (ie. G-actin/SM22).

Chemicals, drugs and enzymes. H-1152, Y-27632, cytochalasin D, and latrunculin A were purchased from Calbiochem (La Jolla, CA). Buffer reagents, collagenases (type F and H), UTP, and 4-AP were obtained from Sigma (St. Louis, MO). Papain was acquired from Worthington (Lakewood, NJ).

Statistical analyses. Data are expressed as means ± S.E., and *n* indicates the number of vessels or cells. Paired t-tests were performed to statistically compare the effects of a given condition/treatment on arterial diameter, E_m, or whole cell current. If more than two conditions or treatments were being compared, a repeated-measures ANOVA was used. When appropriate, a Tukey-Kramer pair-wise comparison was used for post hoc analysis. P values ≤ 0.05 were considered statistically significant.

RESULTS

K_{DR} current and Rho-kinase regulation. To better define the mechanisms enabling pyrimidine nucleotides to inhibit the K_{DR} current, we began our investigation by isolating the current and again demonstrating its susceptibility to UTP inhibition. Using whole-cell patch clamp electrophysiology, the K_{DR} current was readily identified in smooth muscle cells isolated from rat cerebral arteries. As illustrated in Figure 1A, K_{DR} currents were measured by stepping to a series of increasingly positive potentials from a holding potential of -60 mV. The current typically activated at potentials positive to -40 mV and averaged 19.8 ± 1.6 pA/pF at +40 mV. To assess voltage-dependence, tail currents were measured at -40 mV to obtain an accurate indication of the proportion of channels open following a given voltage step. Plotting normalized tail currents against voltage shows activation was detectable at voltages positive to –40 mV and was near maximal at +30 mV (Figure 1B). Applying a Boltzmann function to the data establishes a voltage for half-maximal activation of 3.7 ± 1.0 mV, consistent with previously reported values for the K_{DR} current in cerebral arterial smooth muscle (19; 20).

K_{DR} current amplitude was significantly reduced following the application of UTP (Figure 1C & 1D). As evident in the current-voltage (I-V) relationships, 3×10^{-5} M UTP inhibited the K_{DR} current by 37.0% as measured at +40 mV. This suppression was not associated with changes in whole cell capacitance nor was it attributable to current run-down over time (19). To emphasize that modulation occurs through a Rho-kinase pathway, we measured the effect of UTP following Rho-kinase inhibition (Figure 2). Representative recordings in Figure 2A illustrate that K_{DR} suppression did not occur in the presence of 3×10^{-7} M H-1152, resulting in the absence of any significant net change in the I-V relationship of K_{DR} (Figure 2B). The subsequent addition of the K_V channel blocker 4-AP (5×10^{-3} M) significantly reduced the current (Figures 2A & 2B), verifying the presence of channels known to be regulated by UTP (19). Similar to the effect of H-1152, Rho-kinase inhibition using Y-27632 (3×10^{-5} M) prevented K_{DR} current suppression (*n* = 3; data not shown).

Rho-kinase modulation of the actin cytoskeleton and K_{DR}. To test whether the regulation of K_{DR} current may sequentially involve activation of Rho-kinase and changes in actin structure, we first assayed the state of actin in cerebral arteries following agonist application. Stimulation of unpressurized cerebral arteries with UTP (3×10^{-5} M) induced actin polymerization, eliciting a two-fold increase in the percentage of filamentous (F)

actin (Figure 3A, summary data). Although Rho-kinase inhibition had no significant effect on its own, pre-treatment of vessels with 3 x 10^{-6} M H-1152 prevented UTP-induced polymerization. Although these findings suggest that Rho-kinase is key to the formation of actin filaments during smooth muscle contraction, we were concerned by the markedly low percentage of F-actin observed under control conditions. Further examination revealed that a significant amount of F-actin was present in the pellet fraction following the low speed centrifugation step used to remove cellular debris (Figure 3B), introducing a potential source of error. To more accurately determine changes in actin, we therefore standardized G-actin to SM22, a stable protein also found within the cytosolic fraction. As shown in Figure 3C, normalized G-actin content was significantly reduced following stimulation of vessels with UTP. In contrast, this effect was not observed when arteries were pre-treated with H-1152, verifying that Rho-kinase is essential to the actin dynamics associated with agonist stimulation.

We subsequently monitored the effect of UTP on K_{DR} current following actin disruption. To interfere with actin we first used cytochalasin D, an agent known to depolymerize actin by capping, as well as severing, filamentous actin. Figures 4A & 4C show that the addition of cytochalasin D (1 x 10^{-5} M), despite not having a significant impact on baseline current, completely prevented current suppression by UTP. Similar results were obtained when the experiment was repeated with latrunculin A, which binds globular actin and prevents its incorporation into filaments (Figures 4B). The mean data shows that latrunculin A (1 x 10^{-8} M) did not affect baseline current amplitude but prevented inhibition by UTP (Figure 4D). The substantial block subsequently achieved by 4-AP demonstrates that 4-AP-sensitive channels are present, but not regulated, following actin disruption.

Rho-kinase-mediated depolarization and constriction of cerebral arteries. Given the electrophysiological observations, it would be expected that interfering with either Rho-signaling or actin dynamics would limit the ability of UTP to depolarize and constrict cerebral arteries. As shown in Figures 5A & 5B, arteries preconstricted with UTP dilated to the Rho-kinase inhibitor H-1152 in a concentration-dependent manner. The effect of H-1152 was noticeable at 1 x 10^{-7} M and induced nearly 50% dilation at 3 x 10^{-4} M. We subsequently measured the effect of Rho-kinase inhibition on the ability of UTP to depolarize cerebral smooth muscle. As shown in Figures 5C & 5D, UTP typically depolarized cerebral arteries from a resting E_m of -46.5 ± 1.2 to -32.9 ± 1.9 mV. H-1152

(1 x 10^{-5} M) significantly attenuated the depolarization by 12 mV as E_m was measured at -44.8 ± 3.0 mV. As arteries were stripped of endothelium and maintained at low pressure (15 mmHg), the effects of H-1152 on diameter and E_m were not due to effects on myogenic tone or endothelial-dependent mechanisms.

Role of the actin cytoskeleton in depolarization and constriction. Actin disruption dilated cerebral arteries preconstricted by UTP. As shown in the representative trace and summary data of Figures 6A & 6B, 50% dilation was achieved with 3 x 10^{-6} M cytochalasin D and 1 x 10^{-5} M induced a near complete return to baseline diameter. Membrane potential recordings revealed that cytochalasin D also reversed the depolarization induced by UTP, shifting smooth muscle E_m from -33.2 ± 1.2 to -44.6 ± 3.2 mV (Figure 6C & 6D). In sharp contrast, when we repeated the previous experiment using latrunculin A, we found it affected neither the constriction nor the depolarization associated with UTP (Figure 7). Since latrunculin A disrupts actin by binding G-actin and preventing its incorporation into growing filaments, effects on diameter and electrical responses may not have been detected because agonist-induced alterations in cytoskeletal structure were complete. To address this possibility, we tested whether pre-treatment with latrunculin A may have an effect on agonist responses. The experiment shown in Figure 8A illustrates that a 30 minute pre-incubation with latrunculin A (1 x 10^{-5} M) indeed attenuated the concentration-dependent constriction to UTP. The mean data indicate a significant rightward shift in the sensitivity to UTP (Figure 8B). When vessels were pre-treated with latrunculin A, depolarization to UTP was also significantly attenuated (-37.6 ± 0.9 to -45.5 ± 0.9 mV; Figure 8C & 8D). The above findings are consistent with the idea that disruption of the actin cytoskeleton with cytochalasin D or latrunculin A may limit the extent to which K_{DR} current inhibition contributes to depolarization and constriction.

DISCUSSION

In this study, we further define the mechanisms by which pyrimidine nucleotides elicit constriction of cerebral arteries to effectively reduce blood flow. Electrophysiological examination of smooth muscle cells isolated from cerebral arteries revealed a K_{DR} current that was potently inhibited by UTP through a signaling mechanism involving Rho-kinase. On the basis of previous reports, we questioned whether suppression of the K_{DR} current was dependent on the actin cytoskeleton. We found that Rho-kinase activity was requisite for UTP-induced actin polymerization in cerebral arteries and that interfering with actin dynamics prevented Rho-kinase from regulating the K_{DR} current. The initiation of Rho-kinase-mediated alterations in the cytoskeleton and subsequent inhibition of the K_{DR} current appears to be central in enabling agonists such as UTP to depolarize and constrict cerebral arteries.

K_{DR} current and Rho-kinase regulation. Pyrimidine nucleotides, such as UTP, are endogenous signaling compounds secreted by a number of cell types found in the blood and within the arterial wall (18). When released in close proximity to vascular smooth muscle, pyrimidine nucleotides bind to the P2Y class of receptors to initiate a sustained constriction (7; 15). Cerebral arteries express P2Y2, P2Y4, and P2Y6 receptor subtypes and we have previously investigated the mechanisms enabling UTP to constrict these vessels (19). Detailed examination revealed that smooth muscle depolarization and subsequent voltage-gated Ca^{2+} entry contributed substantially to constriction. We further determined that depolarization was facilitated by the inhibition of an outward K^+ conductance, the K_{DR} current. Consistent with the view that P2Y receptors can couple to $G_{12/13}$ trimeric G proteins to initiate Rho signaling (26), Rho-kinase activity was found to be essential to the suppression of K_{DR} current and to the associated depolarization and constriction.

In the present study we have verified that UTP elicits K_{DR} current inhibition via Rho-kinase. Using conventional whole-cell patch clamp electrophysiology, we readily identified a current with features characteristic of a K_{DR} current: 1) slow time-dependent activation in response to depolarizing potentials, 2) slow deactivation kinetics, and 3) a voltage for half-maximal activation of 3.7 ± 1.0 mV. Additionally, both 4-AP-sensitive and -insensitive components could be distinguished. The 4-AP-sensitive conductance likely includes a heteromultimeric channel formed by Kv1.2, Kv1.5, and Kv1.6 subunits (24), and is of particular relevance as it is the conductance that is regulated by UTP (19). The

4-AP-insensitive current appears to be less susceptible to agonist regulation in the cerebral circulation and may consist of members of Kv2 and Kv7 subfamilies (2; 23).

The stimulation of voltage-clamped cerebral myocytes with UTP elicited K_{DR} current suppression with a magnitude and time-course similar to earlier reports. We have previously implicated Rho signaling in this response, as suppression was abolished following the targeted inactivation of RhoA and Rho-kinase by C3 exoenzyme and Y-27632, respectively (19). Recent studies have demonstrated that Y-27632 can affect PKCδ activity (6; 31), a secondary effect which would complicate our previous interpretation of the ability of Y-27632 to prevent K_{DR} current suppression and arterial depolarization. To address this concern, we opted to use H-1152 as it has been reported to be a more selective and potent Rho-kinase inhibitor (25). H-1152 was found to be more potent than Y-27632, with a concentration of 3×10^{-7} M consistently preventing K_{DR} current suppression in isolated cells. Although both Y-27632 and H-1152 act by competing with ATP-binding to Rho-kinase, the comparable effects of two structurally distinct compounds strengthen the evidence that Rho-kinase is essential in enabling UTP to elicit K_{DR} current suppression. It is apparent that, in addition to the well-described inhibition of myosin phosphatase in Ca^{2+} sensitization, Rho-kinase can also impact ion channel activity.

The actin cytoskeleton and K_{DR} current suppression. Although a dependence on Rho signaling is clear, we questioned the mechanism by which Rho-kinase may influence K_{DR} channel activity. A number of vascular studies have implicated the Rho pathway in the regulation of the cytoskeletal structure, where it can influence both the assembly and disassembly of actin filaments (1; 5; 12; 33). RhoA has been shown to promote actin polymerization by activating profilin, a protein which mediates the addition of actin monomers onto the growing (+) end of filaments (12). Conversely, actin polymerization can also be achieved through a reduced rate of disassembly at the pointed (-) end of actin filaments and this is thought to occur upon activation of the Rho-kinase/LIM-kinase/cofilin pathway (12). We assayed the state of actin and found that Rho-kinase indeed facilitates polymerization in intact cerebral arteries stimulated with UTP. Following stimulation, the percentage of filamentous actin increased and separate analyses of the G-actin content revealed a corresponding decrease. These effects were not observed when arteries were pre-incubated with a Rho-kinase inhibitor prior to agonist application. It may be predicted that such alterations in actin structure would not

only impact smooth muscle cell morphology and force generation, but would likely influence the localization and/or regulation of membrane proteins and signaling complexes, including ion channels. Intriguingly, several K_V channel subtypes thought to contribute to the K_{DR} current, namely Kv1.2 and Kv1.5, have been shown to be capable of associating with actin through cytoskeleton-binding proteins (11; 21).

In the present study, pharmacological disruption of actin with either cytochalasin D or latrunculin A effectively abolished the ability of UTP to suppress K_{DR} current. Therefore, an intact actin cytoskeleton appears essential to Rho-kinase inhibition of the current. Since Rho-kinase promotes actin polymerization, it is likely that alterations in actin structure are associated with changes in cytoskeleton-channel interactions that reduce channel activity. The exact nature of these interactions, and the possible involvement of intermediary proteins, has yet to be resolved. Suppression of the K_{DR} current could also involve channel internalization rather than changes in channel gating. Several reports have indicated that vascular K_{DR} channels may undergo translocation from the membrane to the cytosol in response to agonists (4; 13). The translocation of K_{DR} channels would reduce current density and facilitate arterial depolarization..

Rho-kinase-mediated depolarization and constriction. The functional impact of the preceding mechanism was evident in arterial constrictions to UTP, which displayed a dependence on both Rho-kinase activity and the actin cytoskeleton. Treatment of intact cerebral arteries with H-1152 dilated arteries in a concentration-dependent manner. However, given that Rho-kinase inhibition limits actin polymerization in smooth muscle, part of this dilation is likely due to the disruption of force-generating structures. We therefore directly measured smooth muscle E_m to assess changes in ion channel activity in the absence of effects linked to the force generation. These measurements indicated that Rho-kinase inhibition indeed attenuated UTP-induced depolarization, consistent with an increase in outward conductance that would accompany the relief of K_{DR} current suppression. It should be noted that a significant constriction (~50%) remained following Rho-kinase inhibition, indicating that at least one additional signaling pathway is initiated during constriction to pyrimidine nucleotides. This is not surprising given that UTP is known to elicit Ca^{2+} waves (14), events which have not shown a dependence on Rho signaling.

Similar to the effects of Rho-kinase inhibition, actin disruption using cytochalasin D or latrunculin A limited the electrical and vasomotor responses to UTP. These findings

are congruent with the electrophysiological measurements indicating outward K_{DR} currents are not significantly suppressed under analogous conditions. Intriguingly, the impact of latrunculin A on cerebral vessels depended on the order of application. To observe an effect, vessels had to be pretreated with latrunculin A prior to UTP stimulation. The application of latrunculin A following the agonist response elicited neither a change in E_m nor diameter. We believe these observations reflect the distinct mechanisms by which cytochalasin D and latrunculin A interfere with actin. Cytochalasins are known to cap the growing (+) barbed end of actin and cleave filamentous actin to promote depolymerization, the effects of which become apparent during the sustained response to UTP. In contrast, latrunculin A disrupts actin by binding to globular actin and preventing its incorporation into filaments. As the recruitment of G-actin into filaments is likely complete when a sustained constriction is attained, the subsequent addition of latrunculin would be expected to target residual G-actin with little effect. Although the interconversion between globular and filamentous actin is likely a dynamic process that may promote gradual depolymerization, we did not observe any time-dependent effect of latrunculin over the course of 1-2 hours.

Physiological implications. Our findings indicate that Rho-kinase likely suppresses the K_{DR} current by eliciting reorganization of the cortical actin cytoskeleton. We propose that such a mechanism enables UTP to depolarize smooth muscle, thereby facilitating voltage-gated Ca^{2+} entry and the constriction of cerebral arteries. We have previously hypothesized that pyrimidine nucleotides activate Rho-kinase through the sequential activation of P2Y receptors, $G_{12/13}$, p115 RhoGEF, and RhoA (19). Therefore, cytoskeletal remodeling and K_{DR} current suppression are likely to similarly facilitate depolarization and constriction to uridine diphosphate (19). Furthermore, this type of regulation may not be specific to P2Y receptor agonists as constriction of cerebral arteries to the thromboxane mimetic U46619 also involves Rho-kinase-dependent depolarization (19). Moreover, U46619 elicits a significant suppression of the K_{DR} current (32), conceivably involving a mechanism analogous to UTP inhibition. A role for Rho-kinase in the voltage-dependent constriction of mesenteric arteries has also been reported (8), suggesting the capacity of Rho-kinase to regulate electromechanical coupling extends beyond the cerebral circulation. More detailed examination is required to determine whether the modulation of ion channels and E_m in these tissues is similarly dependent on cytoskeletal remodeling.

In closing, it is clear that the initiation of Rho signaling can alter cerebrovascular tone through multiple, interconnected pathways. In addition to sensitizing the contractile machinery to available Ca^{2+}, Rho-kinase plays an essential role in remodeling the actin cytoskeleton during agonist responses. Our present findings suggest that this influence on actin dynamics enables Rho-kinase to effectively regulate the K_{DR} current and impact electromechanical coupling.

REFERENCES

1. **Albinsson S, Nordstrom I and Hellstrand P.** Stretch of the vascular wall induces smooth muscle differentiation by promoting actin polymerization. J Biol Chem 279: 34849-34855, 2004.

2. **Amberg GC and Santana LF.** Kv2 channels oppose myogenic constriction of rat cerebral arteries. *Am J Physiol Cell Physiol* 291: C348-C356, 2006.

3. **Bhattacharyya R and Wedegaertner PB.** Characterization of G alpha 13-dependent plasma membrane recruitment of p115RhoGEF. *Biochem J* 371: 709-720, 2003.

4. **Cogolludo A, Moreno L, Lodi F, Frazziano G, Cobeño L, Tamargo J, and Perez-Vizcaino F.** Serotonin inhibits voltage-gated K^+ currents in pulmonary artery smooth muscle cells: role of 5-HT2A receptors, caveolin-1, and KV1.5 channel internalization. *Circ Res* 98(7): 931-938, 2006.

5. **Corteling RL, Brett SE, Yin H, Zheng XL, Walsh MP, and Welsh DG.** The functional consequence of RhoA knockdown by RNA interference in rat cerebral arteries. *Am J Physiol Heart Circ Physiol* 293: H440-H447, 2007.

6. **Eto M, Kitazawa T, Yazawa M, Mukai H, Ono Y, and Brautigan DL.** Histamine-induced vasoconstriction involves phosphorylation of a specific inhibitor protein for myosin phosphatase by protein kinase C α and δ isoforms. *J Biol Chem* 276: 29072–29078, 2001.

7. **Garcia-Velasco G, Sanchez M, Hidalgo A, and Garcia de Boto MJ.** Pharmacological dissociation of UTP- and ATP-elicited contractions and relaxations in isolated rat aorta. *Eur J Pharmacol* 294: 521–529, 1995.

8. **Ghisdal P, Vandenberg G and Morel N.** Rho-dependent kinase is involved in agonist-activated calcium entry in rat arteries. *J Physiol* 551: 855-867, 2003.

9. **Harder DR, Alkayed NJ, Lange AR, Gebremedhin D and Roman RJ.** Functional hyperemia in the brain: hypothesis for astrocyte-derived vasodilator metabolites. *Stroke* 29: 229-234, 1998.

10. **Harder DR, Gilbert R and Lombard JH.** Vascular muscle cell depolarization and activation in renal arteries on elevation of transmural pressure. *Am J Physiol Renal Physiol* 253: F778-F781, 1987.

11. **Hattan D, Nesti E, Cachero TG and Morielli AD.** Tyrosine phosphorylation of Kv1.2 modulates its interaction with the actin-binding protein cortactin. *J Biol Chem* 277: 38596-38606, 2002.

12. **Hellstrand P, and Albinsson S.** Stretch-dependent growth and differentiation in vascular smooth muscle: role of the actin cytoskeleton. *Can J Physiol Pharmacol* 83: 869–875, 2005.

13. **Ishiguro M, Morielli AD, Zvarova K, Tranmer BI, Penar PL, and Wellman GC.** Oxyhemoglobin-induced suppression of voltage-dependent K^+ channels in cerebral arteries by enhanced tyrosine kinase activity. *Circ Res* 99(11): 1252-1260, 2006.

14. **Jaggar JH and Nelson MT.** Differential regulation of Ca^{2+} sparks and Ca^{2+} waves by UTP in rat cerebral artery smooth muscle cells. *Am J Physiol Cell Physiol* 279: C1528–C1539, 2000.

15. **Juul B, Plesner L, and Aalkjaer C.** Effects of ATP and UTP on $[Ca^{2+}]_i$, membrane potential and force in isolated rat small arteries. *J Vasc Res* 29: 385–395, 1992.

16. **Kimura M, Dietrich HH, and Dacey RG.** Nitric oxide regulates cerebral arteriolar tone in rats. *Stroke* 25: 2227-2234, 1994.

17. **Knot HJ and Nelson MT.** Regulation of arterial diameter and wall $[Ca^{2+}]$ in cerebral arteries of rat by membrane potential and intravascular pressure. *J Physiol* 508: 199-209, 1998.

18. **Lazarowski ER and Boucher RC.** UTP as an extracellular signaling molecule. *News Physiol Sci* 16: 1-5, 2001.

19. **Luykenaar KD, Brett SE, Wu BN, Wiehler WB and Welsh DG.** Pyrimidine nucleotides suppress K_{DR} currents and depolarize rat cerebral arteries by activating Rho kinase. *Am J Physiol Heart Circ Physiol* 286: H1088-H1100, 2004.

20. **Luykenaar KD and Welsh DG.** Activators of the PKA and PKG pathways attenuate RhoA-mediated suppression of the K_{DR} current in cerebral arteries. *Am J Physiol Heart Circ Physiol* 292: H2654-H2663, 2007.

21. **Maruoka ND, Steele DF, Au BP, Dan P, Zhang X, Moore ED and Fedida D.** Alpha-actinin-2 couples to cardiac Kv1.5 channels, regulating current density and channel localization in HEK cells. *FEBS Lett* 473:188-194, 2000.

22. **Nelson MT and Quayle JM.** Physiological roles and properties of potassium channels in arterial smooth muscle. *Am J Physiol* 268: C799-C822, 1995.

23. **Ohya S, Sergeant GP, Greenwood IA and Horowitz B.** Molecular variants of KCNQ channels expressed in murine portal vein myocytes: a role in delayed rectifier current. *Circ Res* 92: 1016-1023, 2003.

24. **Plane F, Johnson R, Kerr P, Wiehler W, Thorneloe K, Ishii K, Chen T and Cole W.** Heteromultimeric Kv1 channels contribute to myogenic control of arterial diameter. *Circ Res* 96: 216-224, 2005.

25. **Sasaki Y, Suzuki M, and Hidaka H.** The novel and specific Rho-kinase inhibitor (S)-(+)-2-methyl-1-[(4-methyl-5-isoquinoline)sulfonyl]-homopiperazine as a probing molecule for Rho-kinase-involved pathway. *Pharmacol Therap* 93: 225–232, 2002.

26. **Sauzeau V, Le JH, Cario-Toumaniantz C, Vaillant N, Gadeau AP, Desgranges C, Scalbert E, Chardin P, Pacaud P and Loirand G.** P2Y(1), P2Y(2), P2Y(4), and P2Y(6) receptors are coupled to Rho and Rho kinase activation in vascular myocytes. *Am J Physiol Heart Circ Physiol* 278: H1751-H1761, 2000.

27. **Si ML and Lee TJ.** Alpha7-nicotinic acetylcholine receptors on cerebral perivascular sympathetic nerves mediate choline-induced nitrergic neurogenic vasodilation. *Circ Res* 91: 62-69, 2002.

28. **Somlyo AP and Somlyo AV.** Signal transduction by G-proteins, rho-kinase and protein phosphatase to smooth muscle and non-muscle myosin II. *J Physiol* 522: 177-185, 2000.

29. **Somlyo AP and Somlyo AV.** Signal transduction and regulation in smooth muscle. *Nature* 372: 231–236, 1994.

30. **Swärd K, Mita M, Wilson DP, Deng JT, Susnjar M and Walsh MP.** The role of RhoA and Rho-associated kinase in vascular smooth muscle contraction. *Curr Hypertens Rep* 5: 66-72, 2003.

31. **Wilson DP, Susnjar M, Kiss E, Sutherland C, and Walsh MP.** Thromboxane A2-induced contraction of rat caudal arterial smooth muscle involves activation of Ca^{2+} entry and Ca^{2+} sensitization: Rho-associated kinase-mediated phosphorylation of MYPT1 at Thr-855, but not Thr-697. *Biochem J* 389: 763-774, 2005.

32. **Wu BN, Luykenaar KD, Brayden JE, Giles WR, Corteling RL, Wiehler WB, and Welsh DG.** Hyposmotic challenge inhibits inward rectifying K^+ channels in cerebral arterial smooth muscle cells. *Am J Physiol Heart Circ Physiol* 292: H1085-1094, 2007.

33. **Zeidan A, Nordstrom I, Albinsson S, Malmqvist U, Swärd K, and Hellstrand P.** Stretch-induced contractile differentiation of vascular smooth muscle: sensitivity to actin polymerization inhibitors. *Am J Physiol Cell Physiol* 284: C1387–C1396, 2003.

ACKNOWLEDGEMENTS

Operational support was provided by the Canadian Institute of Health Research. K.D. Luykenaar is supported by a doctoral research award provided by the Heart and Stroke Foundation of Canada. D.G. Welsh is a senior scholar with the Alberta Heritage Foundation for Medical Research (AHFMR) and M.P. Walsh is an AHFMR scientist. Both hold a Canada Research Chair.

FIGURE LEGENDS

Figure 1. Delayed rectifier K^+ (K_{DR}) current suppression by UTP in smooth muscle cells isolated from rat cerebral arteries. A: voltage (V) paradigms (top left) were designed to measure steady-state activation. Representative recording of whole-cell K_{DR} current (bottom left). B: plot of steady-state activation. Solid line is a Boltzmann distribution function with half-maximal activation occurring at 3.7 ± 1.0 mV (*n* = 10). C: representative recordings of K_{DR} current before and after the addition of UTP (3×10^{-5} M). D: net I-V relationship (right) under control conditions and in the presence of UTP (*n* = 8). * denotes statistical difference from control.

Figure 2. K_{DR} current suppression by UTP is dependent on Rho-kinase activity. A: representative recordings of the K_{DR} current under control conditions, in the presence of H-1152 (3×10^{-7} M) ± UTP (3×10^{-5} M), and following the addition of 4-AP (5×10^{-3} M). Voltage protocol as in Figure 1. B: net I-V relationship in the presence of H-1152 ± UTP and following the addition of 4-AP (*n* = 6). * denotes statistical difference from control.

Figure 3. UTP induces polymerization of smooth muscle actin through a mechanism dependent on Rho-kinase. A: Western blot (*top*) and summary data (*bottom*) illustrating the effect of H-1152 on actin polymerization in cerebral arteries (*n* = 3). Experiments were performed on unpressurized arteries superfused with physiological salt solution. B: Western blot demonstrating the detection of actin in high speed fractions (G- and F-actin) and in the pellet following low speed centrifugation. C: Western blots detecting actin were re-probed using anti-SM22 antibody (*top*). *Bottom*: Summary data showing the effect of UTP (3×10^{-5} M) ± H-1152 (3×10^{-6} M) on G-actin content after G-actin was standardized to SM22 and normalized to control (*n* = 3). * denotes statistical difference from control.

Figure 4. Disruption of the actin cytoskeleton attenuates the suppression of K_{DR} current by UTP. A: representative recordings of the K_{DR} current under control conditions and in the presence of cytochalasin D (Cyt D; 1×10^{-5} M) ± UTP (3×10^{-5} M). Voltage protocol as in Figure 1. B: representative recordings of the K_{DR} current under control conditions, in the presence of latrunculin A (Lat A; 1×10^{-8} M) ± UTP (3×10^{-5} M), and following the addition of 4-AP (5×10^{-3} M). C: net I-V relationship in the presence of

cytochalasin D ± UTP (n = 6). D: net I-V relationship in the presence of latrunculin A ± UTP and following the addition of 4-AP (n = 6).

Figure 5. UTP-induced depolarization and constriction is dependent on Rho-kinase activity. A: representative trace illustrating the effects of increasing concentration of H-1152 on an artery pre-constricted with UTP. B: summary data of the concentration-dependent effect of H-1152 on a pre-constricted artery (n = 6). C: representative recordings of smooth muscle membrane potential (E_m) measured under control conditions and in the presence of UTP ± H-1152 (1 x 10^{-5} M). D: summary data of E_m measured under control conditions and in the presence of UTP ± H-1152 (n = 6). * and ** denote statistical differences from control and UTP, respectively.

Figure 6. The effect of cytochalasin D (Cyt D) on UTP-induced depolarization and constriction. A: representative trace illustrating the effects of increasing concentration of Cyt D on an artery pre-constricted with UTP. B: summary data of the concentration-dependent effect of Cyt D on a pre-constricted artery (n = 6). C: representative recordings of smooth muscle membrane potential (E_m) measured under control conditions and in the presence of UTP ± Cyt D (1 x 10^{-5} M). D: summary data of E_m measured under control conditions and in the presence of UTP ± Cyt D (n = 6). * and ** denote statistical differences from control and UTP, respectively.

Figure 7. The effect of latrunculin A (Lat A) on UTP-induced depolarization and constriction. A: representative trace illustrating the effects of increasing concentration of Lat A on an artery pre-constricted with UTP. B: summary data of the concentration-dependent effect of Lat A on a pre-constricted artery (n = 6). C: representative recordings of smooth muscle membrane potential (E_m) measured under control conditions and in the presence of UTP ± Lat A (1 x 10^{-5} M). D: summary data of E_m measured under control conditions and in the presence of UTP ± Lat A (n = 6). * denotes statistical difference from control.

Figure 8. The effect of latrunculin A (Lat A) pre-treatment on UTP-induced depolarization and constriction. A: representative trace illustrating the concentration-dependent constriction to UTP in the presence and absence of Lat A. B: summary data of arterial constriction to UTP in the presence or absence of Lat A (n = 6). C: representative recordings of smooth muscle membrane potential (E_m) measured in the

presence of UTP ± pretreatment with Lat A (1 x 10^{-5} M). D: summary data of E_m measured in the presence of UTP ± pretreatment with Lat A (n = 6). * denotes statistical difference.

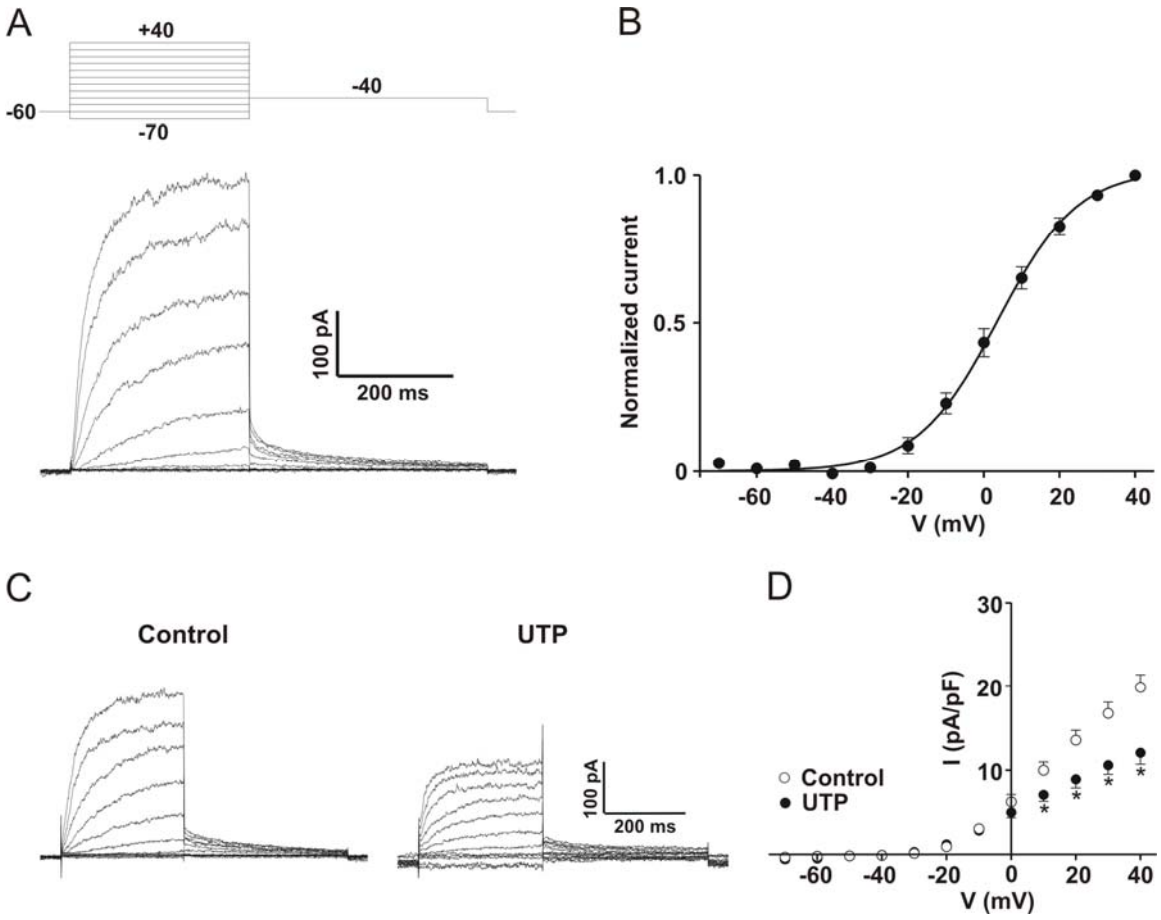
A
+40
-40
-60
-70
100 pA
200 ms
B
Normalized current
1.0
0.5
0
-60
-40
-20
0
20
40
V (mV)
C
Control
UTP
100 pA
200 ms
D
30
20
10
I (pA/pF)
Control
UTP
-60
-40
-20
0
20
40
V (mV)

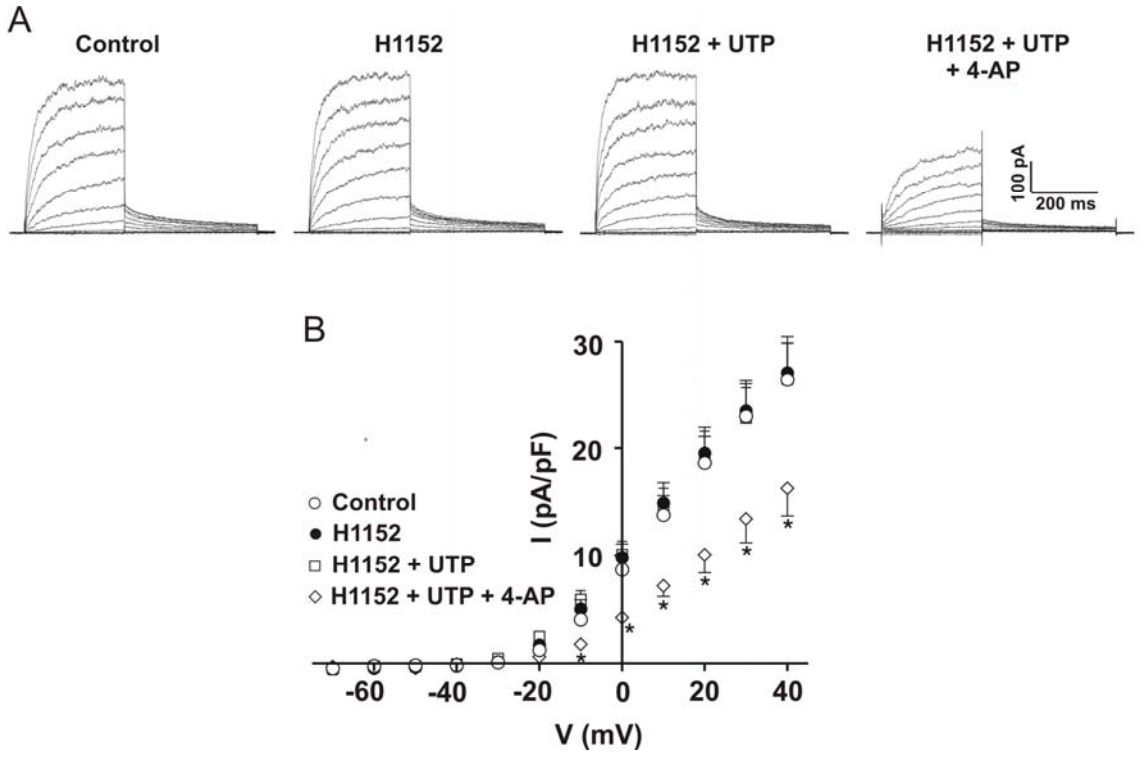
A
Control
H1152
H1152 + UTP
H1152 + UTP
+ 4-AP
100 pA
200 ms
B
Control
H1152
H1152 + UTP
H1152 + UTP + 4-AP
I (pA/pF)
V (mV)
30
20
10
-60
-40
-20
0
20
40

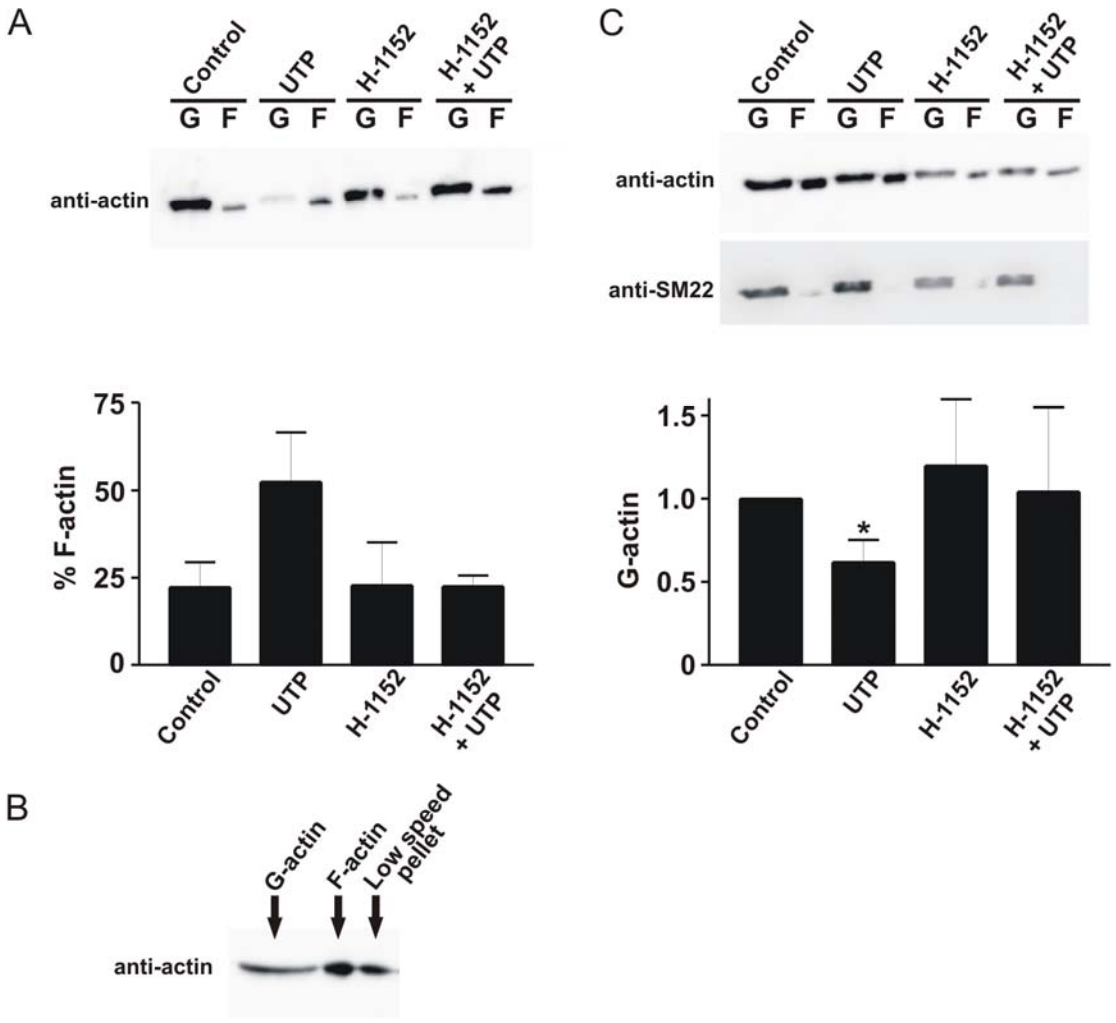
A
Control
UTP
H-1152
H-1152 + UTP
G F G F G F G F
anti-actin
% F-actin
75
50
25
0
Control
UTP
H-1152
H-1152 + UTP
C
Control
UTP
H-1152
H-1152 + UTP
G F G F G F G F
anti-actin
anti-SM22
G-actin
1.5
1.0
0.5
0
*
Control
UTP
H-1152
H-1152 + UTP
B
G-actin
F-actin
Low speed pellet
anti-actin

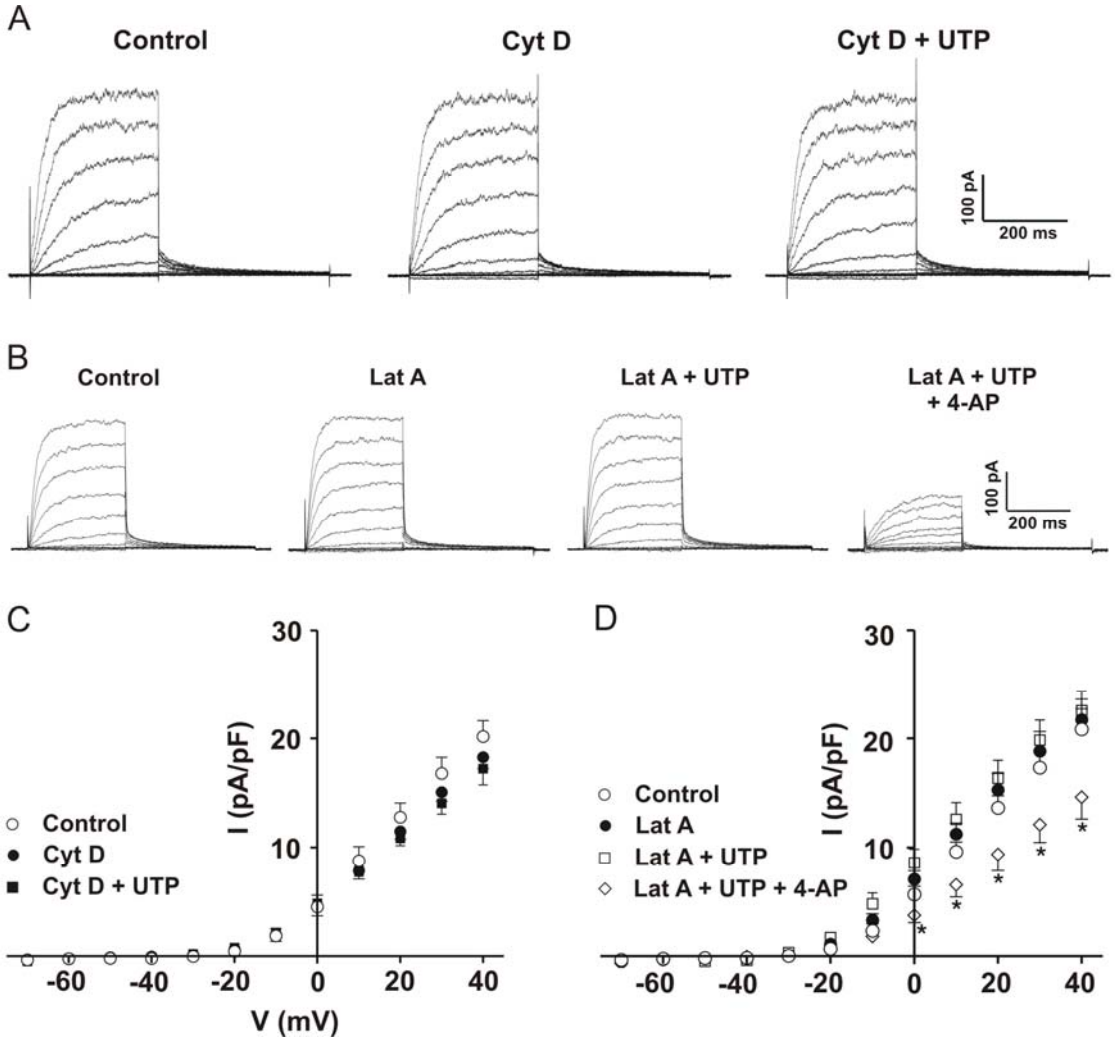
A
Control
Cyt D
Cyt D + UTP
100 pA
200 ms
B
Control
Lat A
Lat A + UTP
Lat A + UTP
+ 4-AP
100 pA
200 ms
C
I (pA/pF)
V (mV)
Control
Cyt D
Cyt D + UTP
D
I (pA/pF)
Control
Lat A
Lat A + UTP
Lat A + UTP + 4-AP

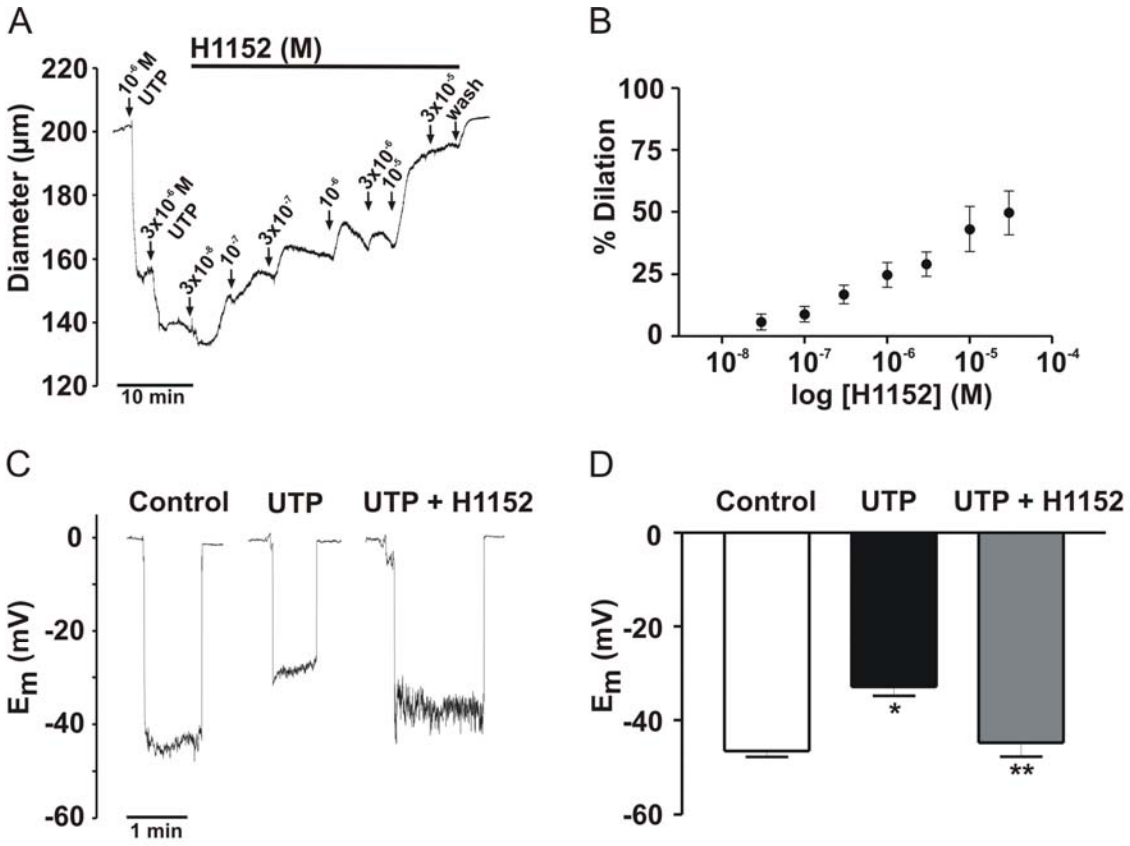
A
H1152 (M)
Diameter (µm)
220
200
180
160
140
120
10 min
B
% Dilation
100
75
50
25
0
log [H1152] (M)
C
Control
UTP
UTP + H1152
Em (mV)
0
-20
-40
-60
1 min
D
Control
UTP
UTP + H1152
Em (mV)
0
-20
-40
-60
*
**

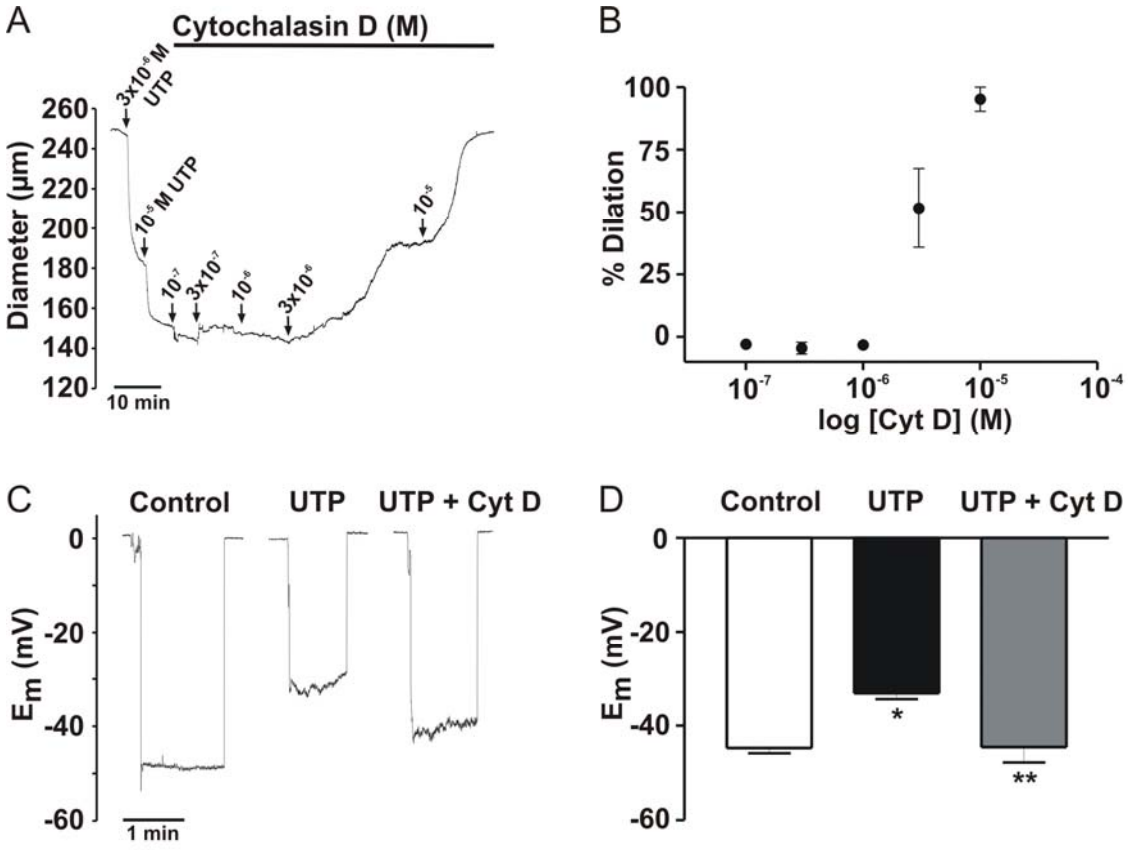
A
Cytochalasin D (M)
3x10⁻⁶M UTP
10⁻⁵M UTP
10⁻⁷
3x10⁻⁷
10⁻⁶
3x10⁻⁶
10⁻⁵
Diameter (µm)
260
240
220
200
180
160
140
120
10 min
B
% Dilation
100
75
50
25
0
10⁻⁷
10⁻⁶
10⁻⁵
10⁻⁴
log [Cyt D] (M)
C
Control
UTP
UTP + Cyt D
Em (mV)
0
-20
-40
-60
1 min
D
Control
UTP
UTP + Cyt D
Em (mV)
0
-20
-40
-60
*
**

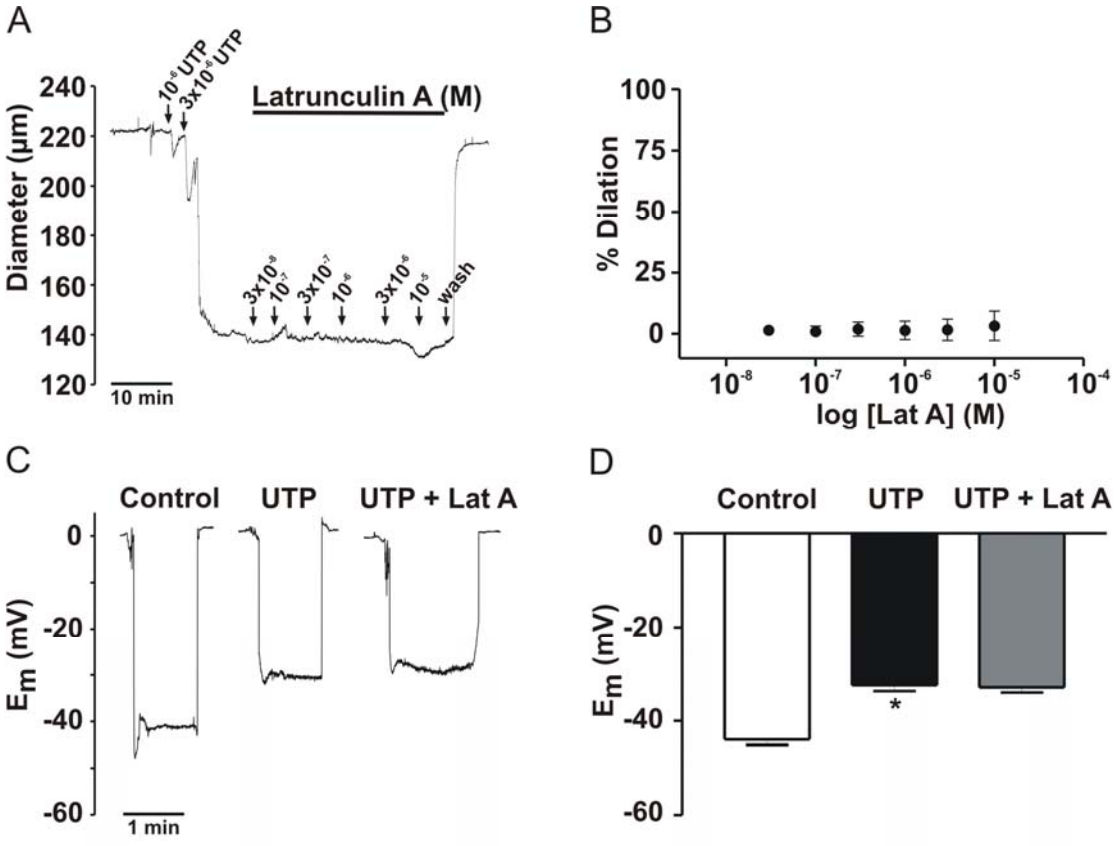
A
Diameter (µm)
240
220
200
180
160
140
120
10 min
10⁻⁶ UTP
3x10⁻⁶ UTP
Latrunculin A (M)
3x10⁻⁸
10⁻⁷
3x10⁻⁷
10⁻⁶
3x10⁻⁶
10⁻⁵
wash
B
% Dilation
100
75
50
25
0
10⁻⁸
10⁻⁷
10⁻⁶
10⁻⁵
10⁻⁴
log [Lat A] (M)
C
Control
UTP
UTP + Lat A
Em (mV)
0
-20
-40
-60
1 min
D
Control
UTP
UTP + Lat A
Em (mV)
0
-20
-40
-60
*

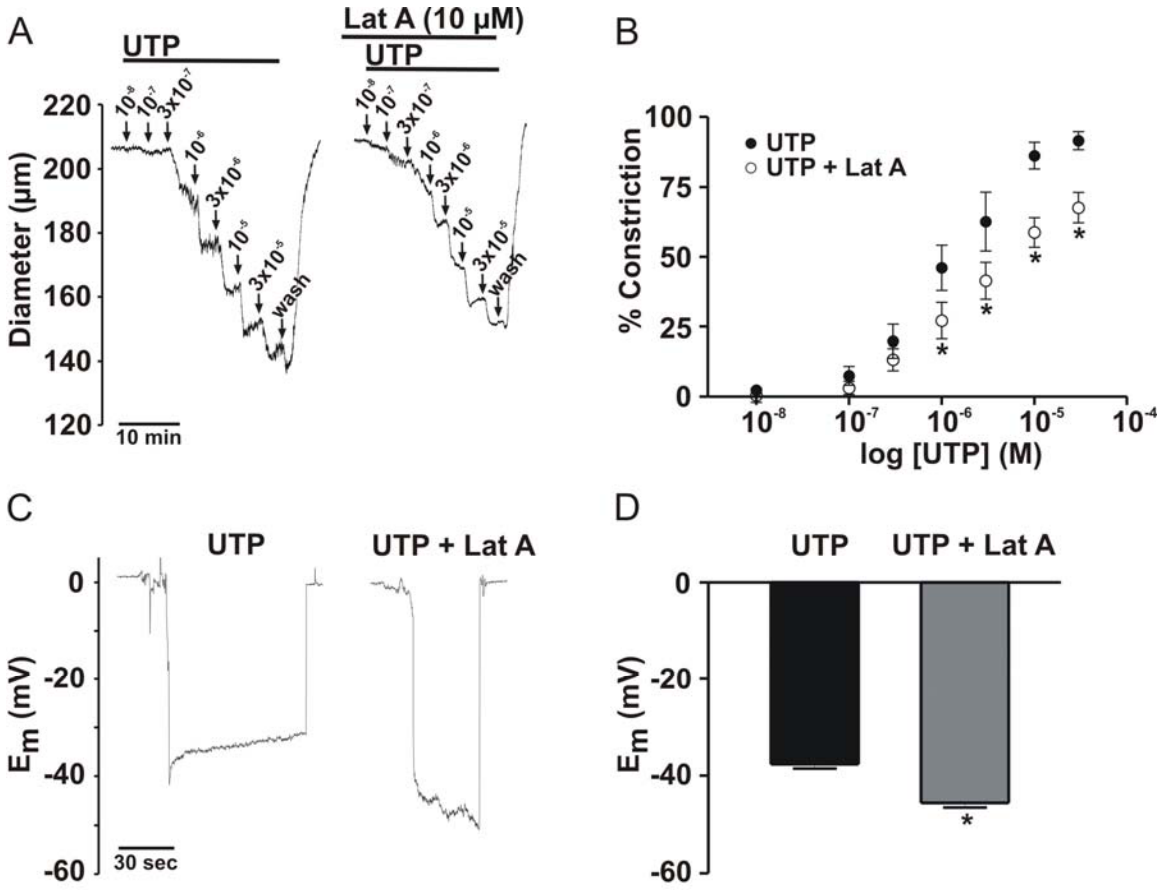
A
UTP
Lat A (10 μM)
UTP
Diameter (μm)
220
200
180
160
140
120
10 min
wash
wash
B
% Constriction
100
75
50
25
0
UTP
UTP + Lat A
log [UTP] (M)
C
UTP
UTP + Lat A
Em (mV)
0
-20
-40
-60
30 sec
D
UTP
UTP + Lat A
Em (mV)
0
-20
-40
-60